Proceedings of the ASME 2022 41st International Conference on Ocean, Offshore and Arctic Engineering
OMAE2022
June 5-10, 2022, Hamburg, Germany

OMAE2022-78557

FREAK WAVE FORECASTING: A DATA-DRIVEN APPROACH

Thomas Breunung
Department of Mechanical Engineering
University of Maryland, College Park, MD, US

Balakumar Balachandran
Department of Mechanical Engineering
University of Maryland, College Park, MD, US

ABSTRACT

Freak waves, waves significantly higher than neighboring waves, are a serious threat to ships and marine infrastructure. Despite significant refinement of operational wave models and recent progress in studying the theoretical foundations of such extreme events, the emergence of these events remains unpredictable. In this work, the authors propose a data-driven wave forecasting approach by combining the essence of common wave models, rapid oscillations, and slowly changing spectrum with data-driven techniques such as recurrent neural networks. A judicious minimization procedure is developed, wherein the sea surface elevation is first decomposed into harmonic functions with varying amplitudes. Then, the amplitude variations are forecasted by fitting universal, black-box models. This approach, which can be used to forecast wave crests and troughs in real time, is tested on available buoy data. Overall, the developed models and fitting strategies outperform simple benchmarks indicating the approach's potential for operational, real-time wave forecasting.

Keywords: Data-driven modelling, extreme waves, forecasting, machine learning

1. INTRODUCTION

Rogue waves are waves with a crest height n_c exceeding the significant wave height H_s by a factor of 1.25 ($n_c/H_s > 1.25$), where H_s is defined as four times the standard deviation of the surface elevation [1,2]. These extreme waves have seriously damaged marine infrastructure, endangered ships, and severely injured humans [3,4]. Hence, reliable ocean wave forecasting is of paramount importance for safe naval operations.

This critical need has inspired a significant research effort to model ocean waves, for example, with spectral wave models [5,6]. The time evolution of wave spectra is governed by an energy balance equation that can be parameterized in various forms. Important terms include the wind input, dissipation, and nonlinear wave interactions. The nonlinear terms, arising through a perturbation series of the ocean wave spectrum, capture resonance interactions between individual wave components [2] and these interactions have been identified as a crucial driving mechanism for wave growth [7]. Such models can yield accurate predictions over multiple days [8]. Such models, however, do not capture non-resonant interactions between waves which can be significant for freak wave occurrence [9]. More importantly, in the energy balance equation, as an underlying governing assumption, one considers a slow variation of the wave spectra over large temporal and spatial (ranging several kilometers) domains. However, this coarse resolution fundamentally limits the use of spectra to model, understand, or forecast inherently localized phenomena such as rogue waves. To illustrate this fact, two 30 minutes recordings of ocean surface elevation measured off the coast of San Nicholas island are shown in Figure 1. While both spectra are very similar, only the recording from January 19, 2019 corresponds to an extreme wave with a crest height of about 5.5 m exceeding the significant wave height of about 3.9 m by a factor of 1.4 (cf. inset in Fig. 1).

Alternatively, ocean waves have been analyzed by using classical equations and perturbation approaches. Building on Stokes' analysis (see, e.g., [11]), ocean waves have been modeled, for example, with the nonlinear Schrödinger equation [4,12,13] and this equation's extensions to include higher order terms (see, e.g., [14]). These analyses reveal the modulation or Benjamin-Feir instability as a possible mechanism for freak wave formation. Additionally, linear focusing and wave-current interactions have been identified as feasible causes. While such simplified models yield valuable insights, the applicability of these models in a more realistic setting is rather limited, since the assumptions of, for example, unidirectionality, stationarity, or a narrow band process do not correspond to reality. Furthermore,

two recent extensive data analyses [15,16] on buoy data have revealed that classical rogue wave indicators such as the Benjamin-Feir index (see, e.g., [17]) do not serve as good predictors for rogue waves.

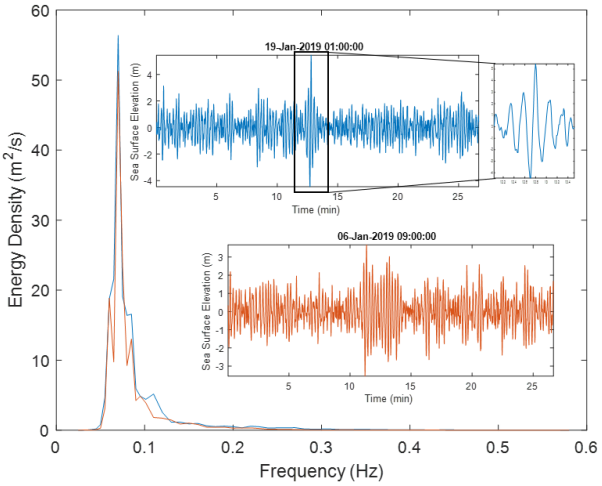

Figure 1: TWO 30 MINTUES OF BUOY RECODINGS OF THE COAST OF SAN NICHOLAS ISLAND (CDIP BUOY 067) YIELDING SIMILAR WAVE SPECTRA. HOWEVER ONLY THE MEASUREMENT FROM JANUARY 19, 2019, CORRESPONDS TO FREAK WAVE. DATA FROM COASTAL DATA INFORMATION PROGRAM (CDIP), SCRIPPS INSTITUTION OF OCEANOGRAPHY [10].

Important insights on the formation of rogue waves can also be deduced from experimental and numerical wave tanks. Such well-controlled idealizations of the ocean aim to uncover fundamental physical processes driving the formation of ocean waves. Notably, higher order spectral method has been shown to accurately mimic an experimental wave tank [18]. Moreover, it can reproduce known extreme waves [19,20]. These computations and others relying on the boundary element method [21], smoothened particle hydrodynamics [22] or harmonic polynomial cell method [23] are expensive, and hence, cannot generate forecasts in real-time. Moreover, such schemes are cannot be straightforwardly applied to the real ocean, since for example the boundary conditions are generally unclear.

In the recent years, an abundance of data-driven approaches to analyze general time series have been proposed (see, e.g., [24] for a review in fluid dynamics). Methods based on the Koopman operator [25], linear embeddings via dynamic mode decomposition (DMD) [26], or recurrent neural networks with long short-term memory cells (LSTM) [27] have promising appeal for universal black-box approaches. However, such methods are fundamentally interpolative. Hence, their applicability for ocean wave forecasting, an extrapolative task, remains unclear. Moreover, the black-box character allows only for limited physical insights, and consequently, these approaches are not amenable for developing a systematic understanding of possible driving mechanisms.

In summary, spectral methods were developed for time and length scales larger than rogue waves, while the analytical models have a limited applicability to real ocean waves. Moreover, data-driven black-box models will suffer from limited interpretability and poor extrapolation. To overcome these limitations, the authors combine the strengths of the aforementioned approaches in this work. Drawing inspiration from the existing wave models, the ocean surface elevation is approximated by rapid oscillations with slowly varying amplitudes. Subsequently, the time evolutions of these amplitudes are forecasted by using linear models and a neural network consisting of LSTM cells. The performance of this approach is demonstrated on buoy data from Coastal Data Information Program (CDIP), Scripps Institution of Oceanography [10]. Overall, an accurate forecasting ability of ocean waves superior to the relevant benchmarks is demonstrated. Moreover, an imminent rogue wave is predicted one minute in advance.

2. MATERIALS AND METHODS

First, the wave model used in this study and the employed procedure to fit parameters to buoy data [10] are described. Subsequently, the authors explain the dynamical models utilized to forecast the model's slowly varying amplitudes. Following that, the forecasting strategy and data processing enabling real-time operational wave forecasting is illustrated.

2.1 Wave model

Persuaded by the continuous up and down movement of the ocean surface, in most analyses, one models the ocean surface as a sum of harmonic functions

$$h_f(t) = \sum_{j=1}^{N} u_j(t)\cos(\omega_j t) + v_j(t)\sin(\omega_j t), \qquad (1)$$

where ω_j are the frequencies and the integer N denotes the number of frequencies. Since available ocean observations reveal a non-constant spectrum of waves, the amplitudes $u_j(t)$ and $v_j(t)$ are allowed to vary in time. It is noted that instead of introducing two amplitudes for each frequency ($u_j(t)$ and $v_j(t)$) one can equivalently introduce a single amplitude and a phase φ_j for each frequency. An advantage of the formulation with two amplitudes is that the model (1) is linear in both amplitudes, whereas an equivalent model to equation (1) formulated with a phase would be nonlinear in the phase variable φ_j.

Although the model (1) is flexible and can be used, at least in principle, to fit any sufficiently smooth function, simplifications are inevitable before using model (1) to fit measurements of the ocean surface. Most importantly, the aim of the work is to forecast forthcoming wave crests and troughs, and hence, intermediate values between wave peaks and troughs are only of secondary interest. Therefore, these intermediate values are discarded and only the crest heights and trough depths are kept for fitting. With this approach, one reduces the number of data points within a time window significantly and thus enables a more accurate fit with the use of less parameters. This filtering yields a nonuniformly spaced discrete time series of crest heights

and trough depths, which is labeled with $h(t_j)$, where t_j denote the time instances.

Most commonly the parameters of model (1) are fitted with the help of the Fourier transform, in particular, the FFT-algorithm, an algorithmic implementation for discrete time series. However, it needs to be noted that the Fourier transformation is defined for infinitely long time series. In contrast, measurements have a finite duration. Thus, in any such computation, one implicitly assumes a continuation of the measured time series outside the measurement window. Most prominent is a periodic continuation of the measured signal or a zero-signal outside the measurement window. In the latter case, the Fourier coefficients are computed by a convolution with an appropriately chosen filter function, for example, the cosine filter. In this work, such assumptions are avoided, by determining the parameters in model (1) through a function optimization. Since the model (1) is nonlinear in the frequencies ω_j, a nonlinear optimization is required. To this end, the cost function

$$\begin{aligned} \mathrm{Z}\left(\omega_j, u_j(t), v_j(t)\right) := & \left\|h(t) - h_f(t)\right\|^2 \\ & + \tfrac{1}{\varepsilon}\textstyle\sum_{j=1}^{N}\left(\left\|\dot{u}_j(t)\right\|^2 + \left\|\dot{v}_j(t)\right\|^2\right) \\ & + \alpha\left\|\textstyle\sum_{j=1}^{N} u_j(t)\omega_j \sin\left(\omega_j t\right) - v_j(t)\omega_j \cos\left(\omega_j t\right)\right\|^2, \end{aligned} \tag{2}$$

is introduced, where $\|\ \|$ denotes the L_2-norm; that is, $\|h(t)\|^2 := \sum h\left(t_j\right)^2$. The first term in equation (1) ensures an accurate fit to the extreme values of measured data.

The second term is used to penalize large variations in the amplitudes $u_j(t)$ and $v_j(t)$. Most observations of ocean surface and physical considerations leading to the energy balance equation [5], the nonlinear Schrödinger equation and its extension [3] or a third order spectral analysis [28] indicate that the time variations of the amplitudes are small. Such a slow variation can be readily enforced by selecting ε in the cost function (2) to be appropriately small.

Moreover, for small time variations of the amplitudes $u_j(t)$ and $v_j(t)$, the last term in equation (2) corresponds to the time derivative of the fitting function (1). Thus, the cost function (2) also requires small time derivatives at the time instances t_j, whereby it is ensured that $h_f(t_j)$ are indeed approximately extreme values, respectively, wave crests or troughs.

The parameters, more specifically, the frequencies ω_j and the amplitudes $u_j(t)$ and $v_j(t)$, are obtained by the minimization

$$\arg\min_{\omega_j, u_j(t), v_j(t)} \mathrm{Z}\left(\omega_j, u_j(t), v_j(t)\right), \tag{3}$$

which is a nonlinear optimization, since h_f(t) is nonlinear in the frequencies ω_j. To reduce the computational burden of the nonlinear function optimization and avoid spurious solutions, a two-step procedure is adapted. In a first step, the amplitudes are kept constant ($u_j(t) = u_j = const$ and $v_j(t) = v_j = const$) and the nonlinear minimization

$$\arg\min_{\omega_j, u_j, v_j} \mathrm{Z}\left(\omega_j, u_j, v_j\right), \tag{4}$$

is numerically solved by using the nonlinear least squares solver 'lsqnonlin' provided in MATLAB. It is observed that the obtained minimum strongly depends on the initialization of the frequencies ω_j. To avoid non-optimal solutions with a large residual, a Monte Carlo method is utilized. The optimization (4) is started from multiple initial frequencies. These initializations are obtained by sampling a uniform distribution in the interval between 0.02 Hz and 0.6 Hz, which corresponds to the frequency interval in which ocean waves are commonly observed (see, e.g., [7]). The determined parameters u_j, v_j and ω_j are taken from the optimization yielding the lowest residual.

After numerically solving the minimization (4), the frequencies ω_j are kept fixed at their values obtained by Monte Carlo sampling and the amplitudes $u_j(t)$ and $v_j(t)$ are allowed to vary in time; that is,

$$\arg\min_{u_j(t), v_j(t)} \mathrm{Z}\left(\omega_j, u_j(t), v_j(t)\right), \tag{5}$$

is solved. Since the cost function $\mathrm{Z}\left(\omega_j, u_j(t), v_j(t)\right)$ is quadratic in the amplitudes $u_j(t)$ and $v_j(t)$, the minimization (5) can be efficiently solved in closed form. Thus, solving the equation (5) is computationally significantly cheaper than the solution strategy adapted for equation (4).

In Figure 2, the authors show an example of an obtained fit for the sea surface elevation over a five-minute window. Five Fourier modes are selected in the model (1) ($N = 5$) and the parameter controlling the slowness of the amplitude variation was set to $\varepsilon = 10^{-3}$. Moreover, $\alpha = 0.5$ was selected and one thousand samples each consisting of five frequencies were drawn to solve the minimization (4). The fitted surface (red) closely resembles the measured data in blue, whereas the amplitudes remain almost constant (small variations) as enforced by the small parameter ε. The relative residual error for the data shown in Figure 2 is about twelve percent. The average relative fitting error of crests heights and trough depths for one hundred randomly selected five-minute windows fitted with the same parameters is 9.8 percent with a standard deviation of 5 percent.

The fitting procedure for the wave model (1) described in this section yields N frequencies ω_j and $2N + 1$ time series of slowly varying amplitudes. To enable ocean wave forecasting with the model (1), the amplitudes $u_j(t)$ and $v_j(t)$ need to be extrapolated beyond the measurement interval to predict future values. To this end, dynamical models are developed in the next section.

2.2 Dynamical models

To enable forecasting, dynamical models are fitted to the time series of the amplitudes $u_j(t)$ and $v_j(t)$ (cf. bottom part of Fig. 2). In the absence of well-established modeling approaches for the slowly varying amplitudes, data-driven black-box models

are used. More specifically, linear autoregressive models and a neural network consisting of LSTM cells [27] are employed here.

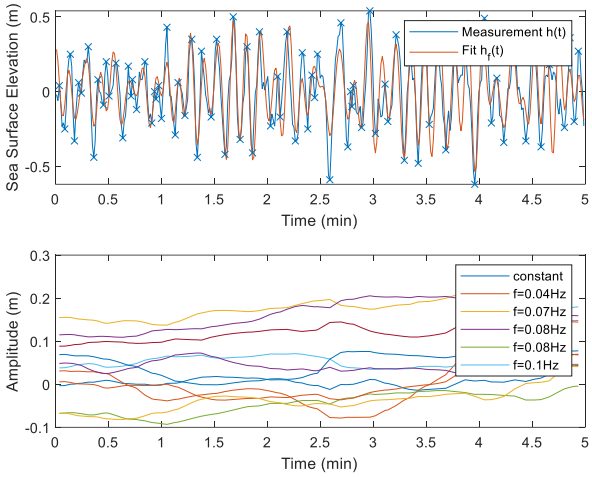

Figure 2: FIT OF THE SEA SURFACE AND TIME DEPENDENT AMPLITUDES OF 5 FOURIER MODES, $\varepsilon = 10^{-3}$, AND $\alpha = 0.5$ (CF. COST FUNCTION (2)).

Time series forecasting generally requires extrapolation and the aforementioned models are interpolative with limited extrapolation capabilities. However, in the setting of this work, the modelling effort of the pervious section becomes beneficial. Comparing the upper and lower plots in Figure 2, one intuitively expects that an extrapolation of the slowly varying lines in the bottom plot is more promising than extrapolation on the rapidly changing ocean surface. Indeed, in this work, a dynamical system is fitted to evolve the slowly varying amplitudes $u_j(t)$ and $v_j(t)$ forward in time. Thus, even a restriction of accurate extrapolations of the slow variations to short time scales (with respect to the slow dynamics) can yield accurate forecasts for the fast variations of the full ocean surface. It is expected that such an approach enables forecasts in a range of minutes, whereas the linear autocorrelation of the ocean surface elevation is close to zero after about four seconds.

2.2.1 LINEAR DYNAMICAL MODELS

Here, the authors utilize linear autoregressive models of the form

$$u_j(t_l) = \sum_{m=1}^{M} \beta_m \, u_j(t_{l-m}), \qquad (6)$$

where the coefficients β_m are scalars and M denotes the order of the autoregressive model. Before, fitting the coefficients to the data, the non-uniform time series of the amplitudes are smoothly interpolated (spline interpolation) to yield the amplitudes $u_j(t)$ and $v_j(t)$ in uniform time steps. Then, the coefficients β_m of the dynamics (6) are obtained with two competing methods. First, they are obtained with a least squares fit, which will be referred to as *LSQ*-model. Alternatively, the coefficients can be obtained from a singular value decomposition of the trajectory matrix [29] yielding the *DMD*-model. It is noted that using another popular method, in which one utilizes the method of moments and solves the Yule-Walker equations [30, 31], yields unsatisfactory results, such as exponentially growing amplitudes.

2.2.2 RECURRENT NEURAL NETWORKS

Recurrent neural networks with LSTM cells have been very effective for regression tasks on sequential data such as time series forecasting [32]. Such machine learning methods are tailored for processing large data sets and the aim is to detect patterns within the provided data. They have been successfully applied to numerous tasks (see, e.g., the review [24] for applications in fluid dynamics or [33] for an early application to ocean waves). The functional input-output relationships of LSTM-cells are nonlinear since LSTM-cells utilize nonlinear functions such as sigmoid and hyperbolic tangent (tanh; see, e.g., [27,32]).

The architecture utilized in this work consists of two hundred hidden units; that is, two hundred LSTM unit-cells in parallel. This layer is followed by a fully connected layer filtering one hundred features from the LSTM layer. To avoid overfitting a dropout layer is included. With this layer, one sets each feature extracted from the fully connected layer to zero with a probability set to 0.1. The weights of the neural network are tuned with a stochastic gradient descent utilizing the Adam optimizer [34].

The capabilities of the two modelling approaches are illustrated in Figure 3. To this end, a twelve-minute window of the ocean surface elevation is decomposed with twelve Fourier modes ($N = 12$ in model (1)). For the cost function (2), the parameters $\varepsilon = 10^{-3}$ and $\alpha = 0.5$ are selected. Two dynamical models, a linear autoregressive model of order $M = 100$ and a LSTM model are fitted for the amplitudes after using data from the whole time interval. Then, initializing each model at about seven minutes, the upcoming samples are predicted by using the dynamical model only. For the example shown in Figure 3, the LSTM model is found to correctly predict the oscillations in the data, whereas the variations decay quickly with the linear model.

It is remarked that meaningful forecasts will significantly differ from the numerical exercise that resulted in Figure 3, primarily, for two reasons. First, for the dynamical system shown in Figure 3, the training data and the testing data were the same. More precisely, the dynamical systems were fitted by using the data for the whole-time interval, notably, also data after seven minutes that is then subsequently 'forecasted'. In reality, however, the time series to be forecasted is unknown and hence cannot be used to fit the model. Second, the time series of the slowly varying amplitudes are also obtained by minimizing the cost function (2) over the whole-time span including the, in reality unknown, future values. Whether the proposed modeling approach is indeed useful cannot be evaluated from the outcome of a single experiment, such as that shown in Figure 3. To this end, a systematic investigation consisting of multiple observation spans and subsequent averaging of the forecasting capability is necessary. Such an analysis is performed in Section 3.

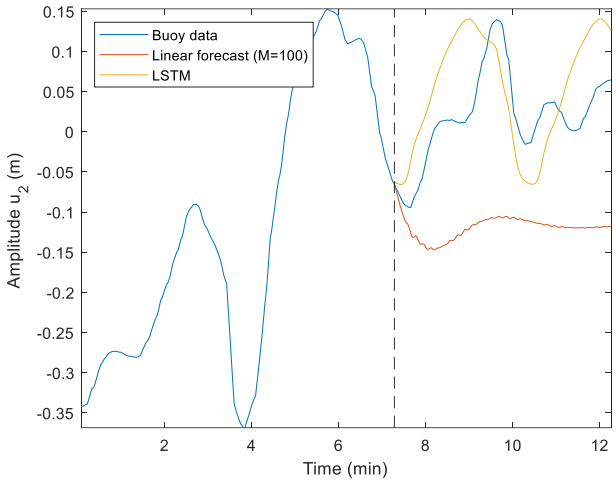

Figure 3: TRUE TIME SERIES, PREDICTION FROM A LINEAR MODEL, AND FORECAST WITH A RECURRENT NEURAL NETWORK WITH LSTM CELLS.

2.3 Forecasting strategy

To enable operational, real-time, wave forecasting the strategy sketched out in Figure 4 is adapted. The durations in Figure 4 are approximative. Their exact values will generally depend on the various parameters involved as well as the underlying buoy data employed for fitting.

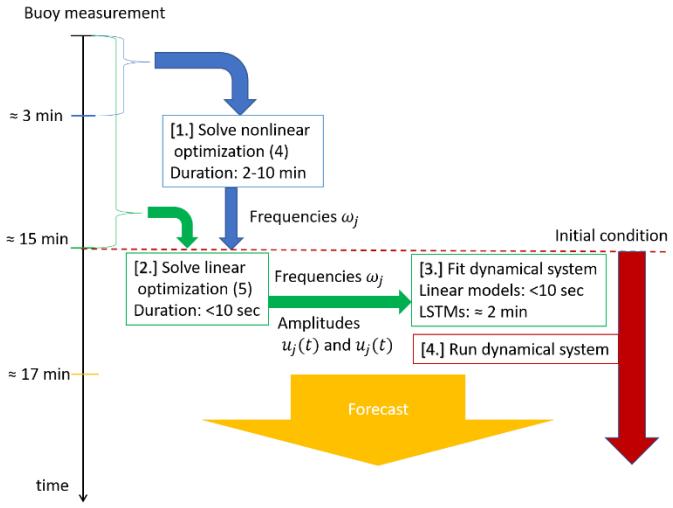

Figure 4: FLOW CHART ENABLING OPERATIONAL, REAL-TIME OCEAN WAVE FORECASTING

As first step, the nonlinear function minimization (4) needs to be solved. Due to the employed Monte Carlo sampling (cf. Section 2.1), this step is computational expensive. To keep this challenge manageable, only a short duration of the buoy data (approx. 3 minutes) is used while solving equation (4). The duration to obtain a solution to equation (4) ranges between two to ten minutes and depends on the number of frequencies in model (1) as well as the number of Monte Carlo samples used.

The frequencies ω_j obtained in the first step are then used in solving equation (5). Since the minimum obtained by solving (5) is available in closed form, this step takes only seconds. To enable real time forecasting, data recorded while solving equation (4) is included when solving the minimization (5). Of course, the frequencies optimized for first three minutes will generally not be the same as fitting frequencies for the whole time interval of approximately 15 minutes. However, as previously mentioned, most wave models as well as observations indicate that the dominant frequencies in the ocean change slowly. Thus, it is reasonable to expect that the dominant frequency components over the first three minutes do not differ significantly from the dominant frequency components over the whole 15-minutes time interval. Indeed, within this work, this expectation can be confirmed. It is observed that solving equations (4) and (5) for the whole 15 minutes of time interval results in only minor improvements compared to the employed strategy (cf. Fig. 4). For example, for $N = 12$ Fourier modes, $\alpha = 0.5$, $\varepsilon = 10^{-3}$, and ten randomly selected 15-minutes windows, the employed strategy yields an average relative mean square error of 3.8% whereas solving equations (4) and (5) for the whole 15 minutes results in a relative mean square error of 3.5%.

Once the time varying amplitudes are known, those are utilized to fit the dynamical systems described in Section 2.2. The coefficients of the linear models are almost instantly available, while the LSTM network requires more time, as the parameter tuning requires minimization of a nonlinear cost function. The last step involves running the fitted dynamical systems to obtain a forecast. The dynamical systems are initialized at the last data point, which is available when fitting their parameters (at about 15 minutes, cf. Figure 4). Thus, about the first two minutes of the obtained time series are not forecasts, since these data points have already passed in reality. After that, the fitted models are used to generate forecasts of ocean surface elevation. The start time and time span of the actual forecast is indicated in yellow in Figure 4.

3. RESULTS AND DISCUSSION

The above described model and forecasting strategy is tested on available buoy data from CDIP, Scripps Institution of oceanography [10]. The measurements are from a Datawell directional waverider MkIII [35] located near San Nicholas Island in the Pacific Ocean. The recordings span the time interval between February 9, 2018 and March 5, 2019. Three models are tested, namely, two linear models and one recurrent neural network with LSTM cells. While the coefficients of one linear model (*LSQ*) are obtained through a least-squares minimization, the other model's parameters (*DMD*) are fitted through a singular value decomposition of the trajectory matrix [29].

First, the fitted models are used to forecast the slowly varying amplitudes. While such forecasts indicate the convergence of the developed models, a forecast of a slowly varying amplitudes is of limited relevance for applications. Thus, these models are subsequently used to forecast the upcoming wave crests and troughs, a more meaningful quantity in practice.

The discussion is concluded with an exploration of the ability of the developed models to forecast an imminent rogue wave.

3.1 Forecasting slowly varying amplitudes

As a first step, the slowly varying amplitudes are forecasted. Such forecasts show that the models have picked up some meaningful signal from the supplied data. To this end, twelve Fourier modes ($N = 12$ in model (1)) have been used to decompose the ocean surface elevation. Moreover, the parameters $\varepsilon = 10^{-3}$ and $\alpha = 0.5$ were selected for the cost function (2).

To indicate the predictive power of the developed models, those are tested against two benchmarks. As a first benchmark, the mean of each slowly varying amplitude is used as forecast value. For a second benchmark, the forecasted value of each amplitude is kept constant at its value at the last known sample. For comparison of the forecasts, the forecasted amplitudes of each of the three models and both two benchmarks are subtracted from the true values of the amplitudes and the L_2 error is computed. Repeating the fitting procedure described in Section 2 for ten randomly selected time windows within the data set yields the results shown in Figure 5. In this figure, the authors show the mean square error of each model relative to the mean square error of the mean guess (left hand side) and the forecasting of the last sample (right hand side). Thus, a relative mean square error below one indicates that the corresponding model can be used to forecast the variations of the amplitudes more accurately than the corresponding benchmark. It is noted that only error values beyond two minutes are forecasts, as the first two minutes have already passed while fitting the parameters of the various models (cf. Section 2).

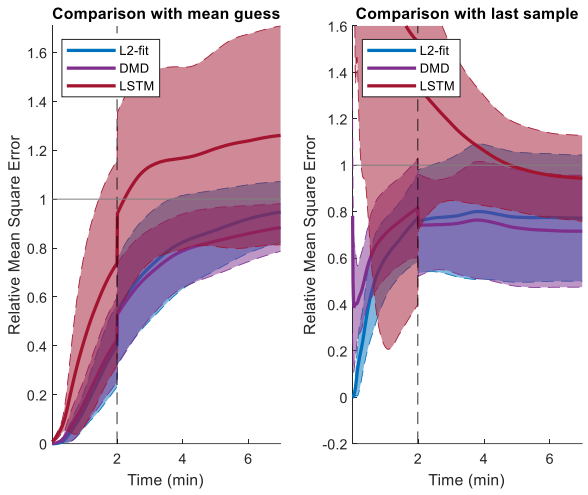

Figure 5: MEAN AND STANDARD DEVIATION OF THE RELATIVE MEAN SQUARE ERROR FOR FORECASTING THE SLOWLY VARYING AMPLITUDES

From Figure 5, it can be discerned that the linear models outperform the mean guess by about twenty percent, whereas the LSTM network does not yield forecasts better than this guess. Comparing with the forecast from the last sample, all three models are found to yield better forecasts, although the performance of the LSTM is only marginally better than the benchmark. Only small differences between the two linear models can be observed in Figure 5.

3.2 Forecasting wave crests and troughs

As a next step, the heights of the forthcoming wave crests and the depths of the upcoming troughs, which are more meaningful quantities in practice, are forecasted. Following the developments from Section 2, the buoy measurements are decomposed into 16 Fourier modes ($N = 16$ in model (1)) and the parameters $\varepsilon = 10^{-3}$ and $\alpha = 0.5$ were selected for the cost function (2). Then, each of the three models is used to generate approximately seven minutes of data, which yields a five-minute forecast of ocean surface elevations (cf. Fig. 4). The wave crest heights and trough depths of the forecasts from the three models are then compared to the actual values. Since peaks and valleys in the forecast and the true data do not occur at the same time instance, not only an error of the forecasted crest heights and trough depths but also in the time when the wave will occur can be computed. Repeating this procedure for one hundred randomly selected windows in the buoy data set, the obtained results are shown in Figure 6.

The three obtained models are compared to a benchmark, which is obtained by forecasting a single wave whose amplitude and period corresponds to the mean values of the training data. In Figure 6, the author show that on the average, linear models predict crest heights and trough depths about 28 cm away from their actual values, whereas the mean error is about 25 cm with the LSTM network. All three models are found to show a significant improvement compared to the benchmark with yields an average error of about 35 cm.

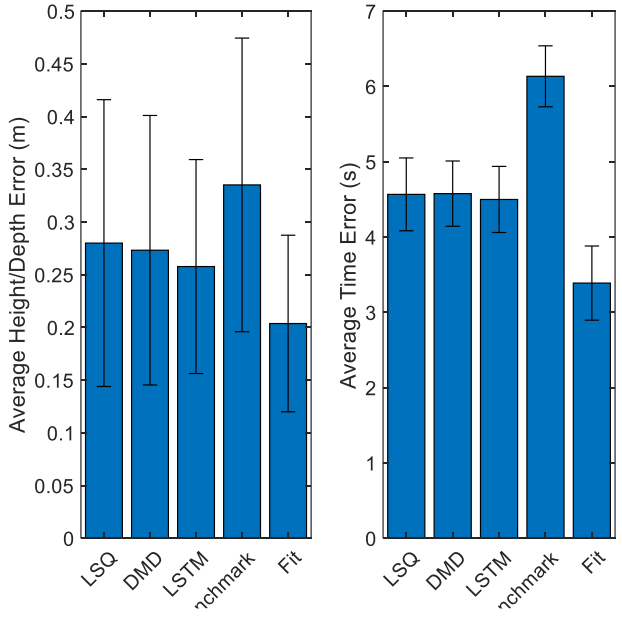

Figure 6: MEAN AND STANDARD DEVIATION OF THE ERROR OF FORECASTED CREST HEIGHTS AND TROUGH DEPTH

To validate the accuracy of the forecasts for large waves, the maximal wave crest height or trough depths is extracted from each forecast included in Figure 6. The large waves are then compared to the true value from the buoy data [10]. The average maximal wave crest or trough depth error for the three different models is shown in Figure 7. With the linear models, one predicts the largest crest height or trough depth with an average error of about 0.6 m, whereas with the LSTM-network, one has an average error of only 0.4 m.

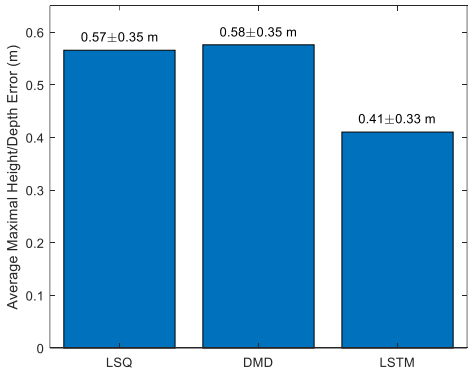

Figure 7: MEAN AND STANDARD DEVIATION OF THE ERROR OF THE FORECASTED MAXIMAL CREST HEIGHT RESPECTIVELY TROUGH DEPTH

3.3 Forecasting a rogue wave

Finally, the developed method is tested to forecast the freak wave shown in the inset in Figure 1. To this end, the buoy measurements are decomposed into 12 Fourier modes ($N = 12$ in model (1)) and the parameters $\varepsilon = 10^{-3}$ and $\alpha = 0.5$ were used in the cost function (2). After fitting the remaining parameters according to the procedure described in Section 2, the obtained LSTM network is used to generate three minutes of data yielding the one-minute forecast shown in Figure 8. Although the full extent of the developing rogue waves is under-estimated by the neural network, the forecast clearly has a significant rise in the peak heights at the rogue wave event up to three meters. The rogue wave is forecasted about one minute in advance from buoy measurements.

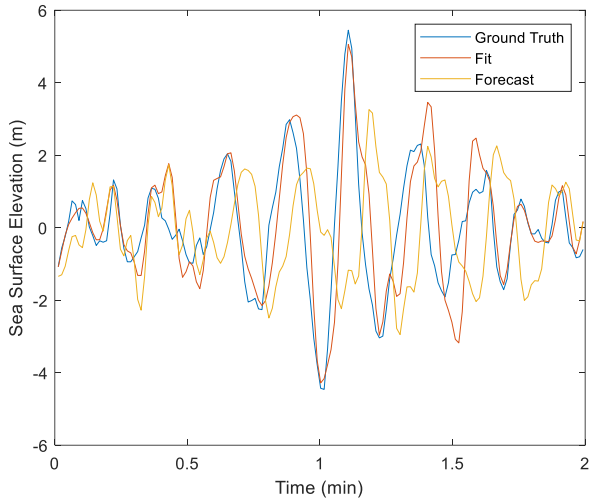

FIGURE 8: FREAK WAVE: GROUND TRUTH , FITTED MODEL AND FORECASTED OCEAN SURFACE ELEVATION

CONCLUSION

In this work, the authors have motivated and proposed the wave model (1) and described a procedure to fit all involved parameters to data. Applying the described procedure to buoy data [10], the obtained models are used for ocean wave forecasting and shown to outperform chosen benchmarks. Moreover, a freak wave event is forecasted about a minute in advance. For future work, the authors envision working on improving the forecast accuracy as well as the forecast horizon. In addition, consideration will be given to using a wavelet description in place of the Fourier series description. Furthermore, a systematic tuning of the various hyperparameters, most importantly the number of Fourier modes, is planned.

ACKNOWLEDGEMENTS

The authors gratefully acknowledge the support of the National Science Foundation Grant No. CMMI1854532. They are also thankful to Samarpan Chakraborty, Samuel Dipasqua, Soheil Feizi, Kayo Ide, and Aya Abdelsalam Ismail of the University of Maryland, College Park, for ongoing discussions on this work. The data [10] were available from the Coastal Data Information Program (CDIP), Integrative Oceanography Division, operated by the Scripps Institution of Oceanography, under the sponsorship of the U.S. Army Corps of Engineers and the California Department of Parks and Recreation. The authors are also appreciative of the comments received from the reviewers.

REFERENCES

[1] Haver S. (2000). Evidences of the existence of freak waves. Proc. Rogue Waves, 2000. Ifremer, 129–140.

[2] Dysthe, K., Krogstad, H. E., & Müller, P. (2008). Oceanic rogue waves. Annual Review of Fluid Mechanics 40, 287-310.

[3] Didenkulova, I. I., Slunyaev, A. V., Pelinovsky, E. N., & Kharif, C. (2006). Freak waves in 2005. Natural Hazards and Earth System Sciences, 6(6), 1007-1015.
[4] Kharif, C., & Pelinovsky, E. (2003). Physical mechanisms of the rogue wave phenomenon. European Journal of Mechanics-B/Fluids, 22(6), 603-634.
[5] Komen, G. J., Cavaleri, L., Donelan, M., Hasselmann, K., Hasselmann, S., & Janssen, P. A. E. M. (1996). Dynamics and modelling of ocean waves.
[6] Tolman, H. L. (1991). A third-generation model for wind waves on slowly varying, unsteady, and inhomogeneous depths and currents. Journal of Physical Oceanography, 21(6), 782-797.
[7] Hasselmann, K. F., Barnett, T. P., Bouws, E., Carlson, H., Cartwright, D. E., Eake, K., ... & Walden, H. (1973). Measurements of wind-wave growth and swell decay during the Joint North Sea Wave Project (JONSWAP). Ergaenzungsheft zur Deutschen Hydrographischen Zeitschrift, Reihe A
[8] Cavaleri, L., Alves, J. H., Ardhuin, F., Babanin, A., Banner, M., Belibassakis, K., …, & Young, I. (2007). Wave modelling–the state of the art. Progress in oceanography, 75(4), 603-674.
[9] Janssen, P. A. (2003). Nonlinear four-wave interactions and freak waves. Journal of Physical Oceanography, 33(4), 863-884.
[10] CDIP Buoy data https://doi.org/10.18437/C7WC72
[11] Dingemans, M. W. (1997). Water wave propagation over uneven bottoms: Linear wave propagation (Vol. 13). World Scientific.
[12] Wang, R., & Balachandran, B. (2018). Extreme wave formation in unidirectional sea due to stochastic wave phase dynamics. Physics Letters A, 382(28), 1864-1872.
[13] Farazmand, M., & Sapsis, T. P. (2019). Extreme events: Mechanisms and prediction. Applied Mechanics Reviews, 71(5).
[14] Dysthe, K. B. (1979). Note on a modification to the nonlinear Schrödinger equation for application to deep water waves. Proceedings of the Royal Society of London. A. Mathematical and Physical Sciences, 369(1736), 105-114.
[15] Cattrell, A. D., Srokosz, M., Moat, B. I., & Marsh, R. (2018). Can rogue waves be predicted using characteristic wave parameters?. Journal of Geophysical Research: Oceans, 123(8), 5624-5636.
[16] Häfner, D., Gemmrich, J., & Jochum, M. (2021). Real-world rogue wave probabilities. Scientific Reports, 11(1), 1-11.
[17] Janssen, P. A. E. M., & Bidlot, J. R. (2009). On the extension of the freak wave warning system and its verification. European Centre for Medium-Range Weather Forecasts.
[18] Toffoli, A., Gramstad, O., Trulsen, K., Monbaliu, J., Bitner-Gregersen, E., & Onorato, M. (2010). Evolution of weakly nonlinear random directional waves: laboratory experiments and numerical simulations. Journal of Fluid Mechanics, 664, 313-336.
[19] Bitner-Gregersen, E. M., Fernández, L., Lefèvre, J. M., Monbaliu, J., & Toffoli, A. (2014). The North Sea Andrea storm and numerical simulations. Natural Hazards and Earth System Sciences, 14(6), 1407-1415.
[20] Bitner-Gregersen, E. M., Gramstad, O., Magnusson, A. K., & Sames, P. (2020). Occurrence frequency of the triple rogue waves in the ocean. In Proc. OMAE 2020 Conf., Fort Lauderdale, FL, USA
[21] Fochesato, C., Grilli, S., & Dias, F. (2007). Numerical modeling of extreme rogue waves generated by directional energy focusing. Wave motion, 44(5), 395-416.
[22] Chakraborty, S., & Balachandran, B. (2021). Wave Propagation Studies in Numerical Wave Tanks with Weakly Compressible Smoothed Particle Hydrodynamics. Journal of Marine Science and Engineering, 9(2), 233.
[23] Zhao, B. B., Zheng, K., Duan, W. Y., Ertekin, R. C., & Shao, Y. L. (2020). Time domain simulation of focused waves by High-Level Irrotational Green–Naghdi equations and Harmonic Polynomial Cell method. European Journal of Mechanics-B/Fluids, 82, 83-92.
[24] Brunton, S. L., Noack, B. R., & Koumoutsakos, P. (2020). Machine learning for fluid mechanics. Annual Review of Fluid Mechanics, 52, 477-508.
[25] Rowley, C. W., Mezić, I., Bagheri, S., Schlatter, P., & Henningson, D. S. (2009). Spectral analysis of nonlinear flows. Journal of fluid mechanics, 641, 115-127.
[26] Schmid, P. J. (2010). Dynamic mode decomposition of numerical and experimental data. Journal of fluid mechanics, 656, 5-28.
[27] Hochreiter, S., & Schmidhuber, J. (1997). Long short-term memory. Neural computation, 9(8), 1735-1780.
[28] Hasselmann, K. (1962). On the non-linear energy transfer in a gravity-wave spectrum Part 1. General theory. Journal of Fluid Mechanics, 12(4), 481-500.
[29] Broomhead, D. S., & King, G. P. (1986). Extracting qualitative dynamics from experimental data. Physica D: Nonlinear Phenomena, 20(2-3), 217-236.
[30] Yule, G. (1927). On a method of investigating periodicities in disturbed series, with special reference to Wolfer's sunspot numbers. Philosophical Transactions of the Royal Society of London Series A, 226, 267-298.
[32] Walker, G. T. (1931). On periodicity in series of related terms. Proceedings of the Royal Society of London. Series A, Containing Papers of a Mathematical and Physical Character, 131(818), 518-532.
[33] Goodfellow, I., Bengio, Y., & Courville, A. (2016). Deep learning. MIT press.
[34] Agrawal, J. D., & Deo, M. C. (2002). On-line wave prediction. Marine structures, 15(1), 57-74.
[35] Kingma, D. P., & Ba, J. (2014). Adam: A method for stochastic optimization. arXiv preprint arXiv:1412.6980.
[36] Datawell Directional Waverider MkIII https://www.datawell.nl/Portals/0/Documents/Brochures/datawell_brochure_dwr-mk3_b-09-09.pdf